INSTITUTE OF PHYSICS PUBLISHING NANOTECHNOLOGY
Nanotechnology **16** (2005) 133–136 doi:10.1088/0957-4484/16/1/027

Incident angle dependence of nanogap size in suspended carbon nanotube shadow lithography

Nitin Chopra[1], Wentao Xu[2], Lance E De Long[2] and Bruce J Hinds[1]

[1] Department of Chemical and Materials Science, University of Kentucky, Lexington, KY-40506, USA
[2] Departments of Physics, University of Kentucky, Lexington, KY-40506-0055, USA

E-mail: bjhinds@engr.uky.edu

Received 7 October 2004, in final form 10 November 2004
Published 10 December 2004
Online at stacks.iop.org/Nano/16/133

Abstract
Suspended nanotubes or nanowires can be used in line-of-sight depositions to produce nanometre-scale lines. Reported here is the experimental quantification of line-of-sight shadow widths for multiwalled carbon nanotubes that are suspended (400 nm) over a silicon nitride (Si_3N_4) membrane (transmission electron microscopy) TEM grid by a lithographically defined resist line array. Aluminium evaporation was performed at incident angles of 0.7°–2.0° by use of the slit (0.81 mm diameter). Shadow widths and carbon nanotube diameters were directly observed by scanning transmission electron microscopy (STEM). Observed gaps were less (0–7 nm) than that predicted from simple line-of-sight geometry. Thus, surface migration assisted by the momentum of incident metal evaporant may be an important mechanism in nanoscale shadow lithography processes.

High resolution lithography techniques are required to incorporate isolated molecules into functional, scalable electronic devices. Significant progress has been made in UV and e-beam lithography for reliable deca-nanometre-scale feature sizes [1–3] but scaling to the 1–2 nm molecular size range remains a significant challenge, especially concerning the serial nature of electron beam and scanning probe techniques. Notable success has been achieved in making 2–5 nm junctions to isolate single molecules [4] and nanoparticles [5] for transport studies. These techniques relied on break junctions and direct e-beam writing that have significant challenges in their reliable scaling for device integration. Although carbon nanotubes (CNTs) and nanowires have nanometre-scale diameters, they also have micron-scale lengths; thus, in principle they can be manipulated with current microelectronic fabrication techniques, i.e. photolithographic based patterns. By utilizing randomly dispersed CNTs [6–8] or with electric field alignment [9–11] as shadow masks, nanometre-scale lines have been demonstrated. In addition to CNTs, semiconductor or oxide nanowires can be applied to nanometre-scale gap formation through lift-off [12] or ion beam milling [13]. In both cases it is critical to control placement and diameter control of the nanowires and nanotubes. Another promising line-of-sight technique has also been demonstrated in depositions between hexagonal closest packing of dispersed polystyrene beads [14]. Shadow lithography also makes it possible to readily incorporate self-assembled nanostructures into VLSI processes, in contrast with break junctions [15] and other sequential scanning-probe nanolithography techniques.

Major challenges associated with CNT shadow mask fabrication include control of the diameter and spatial placement of the CNTs. These can be achieved by precisely patterning the catalyst support layer in a chemical vapour deposition growth of multi-wall CNTs (MWCNTs), where the catalytic film thickness controls the resultant MWCNT diameter [16, 17]. Moreover, individually suspended CNTs attached to the tops of photolithographically defined posts have been demonstrated [18]. CNTs have also been aligned by electric field generated between electrodes, and then used to form shadows [9, 11]. However, previous experiments pointed to the difficulty of determining the precise size of

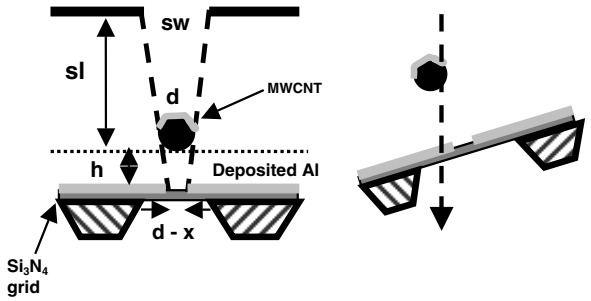

Figure 1. Incident angle dependence of shadow formation under suspended MWCNT. STEM can image both the MWCNT and shadow by tilting the sample. The left-hand diagram shows the deposition geometry, and the right-hand diagram shows the scheme for electron beam imaging. See the text for an explanation of the dimensional parameters.

lines or systematically varying incident deposition angle. Of particular interest is the need to determine if there is significant deviation from line-of-sight geometry due to surface migration of the deposited atoms. By varying incident angle, the role of evaporant momentum can be examined. Previous studies using shadows cast on STM tips revealed a significant 1–20 nm surface migration from ideal line-of-sight geometry [19, 20]. In the case of low temperature Xe deposition, the evaporant impact momentum has a significant effect on migration [19]; while in the case of Sb, thermally excited isotropic surface migration to reduce shadow dimensions is the dominant mechanism [20].

Unfortunately, scanning tunnelling microscopy (STM) or atomic force microscopy (AFM) cannot be used to image either the suspended wire or its shadow, since the suspended wire will interfere with the scanning probe measurements. TEM has high spatial resolution, but sample preparation without damaging the suspended structure is difficult. Here we report a novel approach to put nanoscale patterns directly onto an electron-transparent substrate, allowing for the observation of both the suspended nanotube and the resultant shadow after metal deposition. This analytical sample preparation approach can be used to validate numerous nanofabrication methods. Deviation from line-of-sight geometry can also be studied as a function of incident angle.

The general experimental approach is diagrammed in figure 1. CNTs are suspended above a silicon nitride (Si_3N_4) membrane substrate by dispersing them over an array of thin parallel lines of resist patterned by electron beam lithography. The incident angle of evaporant is controlled by placing a slit at different distances from the sample. The nanotubes and shadow pattern are readily observed via TEM with the sample tilted with respect to incident electron beam. Poly(methyl methacrylate) (PMMA) strip arrays were fabricated by electron beam lithography. The PMMA (MW 495 K, 400 nm thick) was spin-coated onto a silicon nitride membrane window (SPI Supplies, Si_3N_4 thickness of 30 nm) and oven-baked at 165 °C for 3 h. A very thin layer (< 10 nm) of Au was sputter-deposited over the PMMA to reduce charging. The samples were then patterned with a Raith 50 Electron Beam Writer System operated at 30 kV, and then developed in methyl isobutyl ketone (MIBK). The pattern consisted of a simple strip array of parallel lines of 200 nm width and 600 nm pitch. MWCNTs are produced by chemical vapour deposition (CVD) [21] and dispersed into a surfactant [22] (sodium dodecylbenzene sulfonate (NaDDBS)) solution. Individual MWCNTs were randomly dispersed on top of the patterned Si_3N_4 membrane window by dipping the membrane into an MWCNT solution eight to ten times, followed by a rinse in DI water (eight to ten times), and air drying.

Line-of-sight aluminium (Al) deposition was carried out in an e-beam evaporator (Torr International Inc.) on a patterned Si_3N_4 membrane with randomly dispersed MWCNT. The base pressure in the evaporator was between 4.1×10^{-7} and 7.7×10^{-7} Torr. The evaporated metal was only allowed to pass through a 0.81 mm diameter slit placed between the target and substrate. The distance between source and substrate is ∼11.5 cm. A line from the centre of the source through the slit gives an offset angle of 5.71° to the substrate normal. The incident angle that reduces CNT shadow width is determined by slit width and distance as diagrammed in figure 1. The depositions were performed for three different positions of the slit (distance between slit and substrate (sl) ∼2, 5, 7 cm) to control the incident angle of evaporation. The deposition rate was about 0.3 Å s^{-1} in each case. Shadow gaps were directly characterized by scanning transmission electron microscopy (STEM) and energy dispersive spectroscopy (EDS), using a JEOL F2010 operated at 200 keV with ES vision control software. The EDS probe size was 0.5 nm with a 10 s dwell time. Since a quartz crystal monitor cannot be used with slit arrangements, the Al thickness was found by using the atomic ratio of Si and Al from the EDS signal, the known nitride thickness (30 nm) and known material densities. Values of Al thickness of 13, 17, and 21 nm were observed at slit distances of 2, 5, and 7 cm, respectively.

Figure 2 shows an SEM image of the sample geometry and an Al shadow underneath a suspended CNT. The line-of-sight shadow width can be calculated using the geometry of similar triangles from figure 1 and the following equations:

$$(sw - d)/sl = x/h \tag{1}$$

$$w_{\text{gap}} = d - x \tag{2}$$

where sw is the slit width (0.81 mm), sl is the distance between the slit and the suspended MWCNT (2–7 cm), w_{gap} is the gap width, d is the MWCNT diameter, x is the shadow width reduction, and h is the height of the MWCNT above the substrate (resist thickness). Shadow gaps were directly characterized by STEM in order to accurately quantify the dimensions of the gap and the diameter of the MWCNT. Gaps as small as 6 nm (figure 2(B)) were observed for smaller MWCNTs of approximately 20 nm diameter, though most MWCNTs were 40–100 nm in diameter. STEM with x-ray chemical analysis was employed to accurately quantify the dimensions of the gap. Figure 3 shows the dark-field image of a suspended MWCNT and its shadow gap, where the sample is tilted by 15°, permitting the imaging of both the CNT and shadow gap. The dashed line shows the track of an EDS line scan (0.5 nm spot size), and the resulting signals from Si, Al, and C. As expected, the Al signal is reduced to zero in the shadow gap, and a doubling of the Al film signal was observed over the MWCNT, since the electron beam simultaneously goes through Al deposited on top of the MWCNT and through

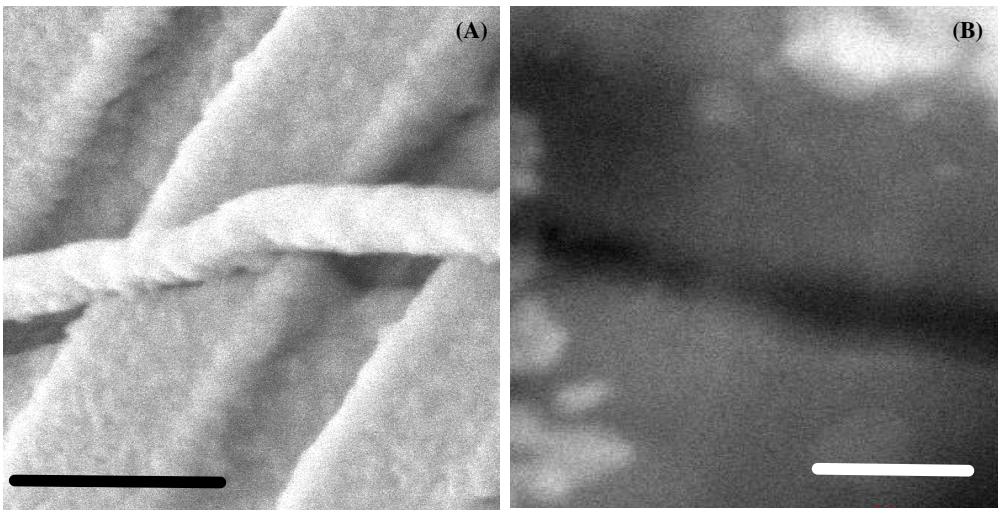

Figure 2. (A) SEM image of an MWCNT suspended on a patterned substrate after Al deposition, showing a shadow underneath the MWCNT. The scale bar is 300 nm. (B) 6 nm shadow projected under a ∼20 nm diameter MWCNT, as seen by STEM. The scale bar is 20 nm.

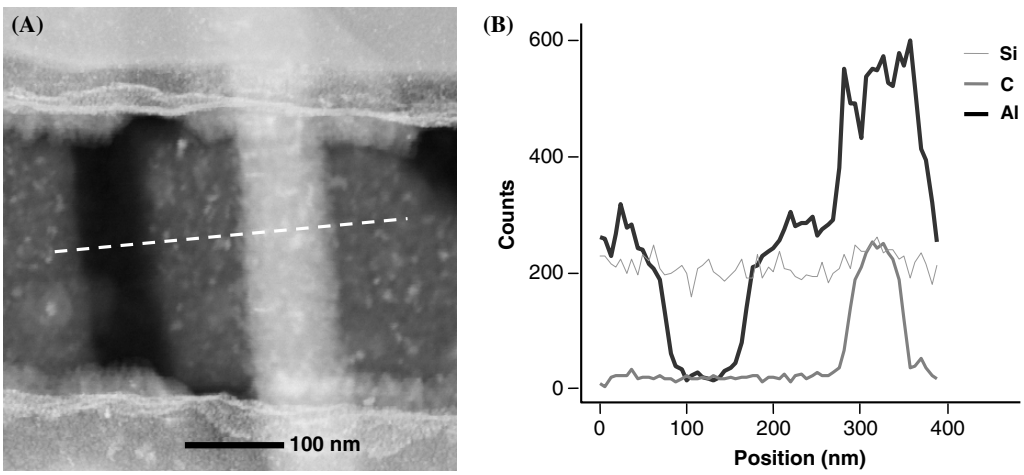

Figure 3. Representative (A) STEM image and (B) EDS line scan (dashed line in (A)) for suspended CNT shadow lithography. The TEM substrate is tilted by 15° relative to the electron beam axis so as to image both the MWCNT and its shadow gap. The evaporation shutter distance was 7 cm; the e-beam resist thickness was 400 nm.

the underlying film when the sample is tilted. The Si signal from the Si_3N_4 membrane substrate remains constant, showing minimal adsorption effects in quantification. Since Al is deposited on top of the MWCNT, the imaged diameter of the MWCNT coated with Al is larger than the MWCNT alone. Hence, a more accurate measure of the CNT diameter is to look at the C signal in the EDS line scan. Gap widths were found by noting where the Al signal went to zero, and the CNT diameter was found by noting the start of the C signal. The gap width is divided by the cosine of the sample tilt angle to correct for the projection geometry of the STEM imaging. Since the MWCNT is cylindrical, no geometric correction is needed. At least six CNT/shadow images were analysed for each incident evaporation angle. Though the diameter of each MWCNT was different, the MWCNT diameter minus shadow width ($x = d - w_{\mathrm{gap}}$) is found to be independent of the MWCNT diameter. It is important to note that during aluminium deposition the effective CNT diameter is increasing and subsequent deposition would have increased the 'gap width'. However, we are measuring where the EDS signal reaches baseline, thus the observed gap width at the initial stages of deposition. The shape of the EDS profile does decrease as it approaches the gap which is consistent with the CNT + Al diameter increasing at later times.

Table 1. Summary of observed gap-width reductions in CNT shadow lithography. The standard deviation for x_{observed} is obtained from the analysis of six different CNT/shadows systems.

Slit distance (sl) (cm)	Incident angle (deg)	x_{calc} (nm)	x_{observed} (nm)	$x_{\mathrm{obs}} - x_{\mathrm{calc}}$ (nm)
7 ± 0.02	0.66 ± 0.004	4.63 ± 0.02	4.2 ± 0.43	-0.43
5 ± 0.008	0.93 ± 0.005	6.48 ± 0.03	10.2 ± 2.6	3.72
2 ± 0.05	2.32 ± 0.05	16.20 ± 0.36	23.6 ± 4.9	7.40

Table 1 and figure 4 summarize observed shadow gap parameters, which are found to be close to values expected from line-of-sight geometry. A reduction in gap width (x) of 4–23 nm is observed as the incident angle is increased

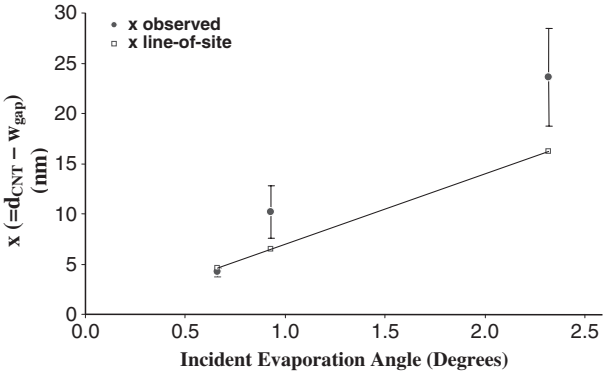

Figure 4. CNT diameter (d_{CNT}) minus shadow width (w_{gap}) versus incident evaporation angle.

from 0.7°–2.0°. Importantly, as incident evaporation angle increases, the pattern is further reduced from that of line-of-sight geometry by roughly 3 nm/deg at these low angles. This suggests that the momentum of incident evaporant atoms is a significant factor that must be taken into account in shadow depositions, and is consistent with previous low temperature STM observations of Xe atoms [19]. In this study the independent variable is incident angle, which would directly affect incident momentum relative to the substrate normal. Other variables such as pressure, deposition rate, and the material/interface energy are presumably kept constant. The degree of migration is also sensitive to deposition atom/substrate interaction. For example, very large (70 nm) migration is seen for Sb on Si at room temperature [20]. The results here with Al are comparable to Cu shadows cast on W field emission tips with 7–9 nm migration past the shadow edge [23]. However, these studies did not use highly collimated sources, thus direct quantitative comparison was not possible.

Suspended MWCNT arrays can cast highly controlled nanometre-scale shadows having dimensions that are very close to line-of-sight geometry. By controlling the incident angle, the suspended nanotube geometry allows the use of *deca-nanometre-diameter* wires to draw nanometre-scale lines. Numerous synthetic strategies to produce semiconductors, oxide and MWCNT with deca-nanometre diameters are reported, and can thus be incorporated into this geometry. Another advantage of the suspended nanowire geometry is that it allows thicker depositions than is the case with contact mask shadows [7], because nanotubes must be subsequently removed from the substrate, making it difficult to deposit films thicker than a nanotube diameter. The suspended geometry also allows CNTs to be located away from the active device area which is in the shadow gap. Gap widths that deviate from line-of-sight geometry suggest that incident momentum can reduce the shadow gap width, hence collimated deposition sources are needed. Further control and detailed analysis of this incident momentum hypothesis can be accomplished by use of rotating shutters (time of flight) to determine the atom's momentum relative to the substrate surface. The method of producing nanostructures directly on Si_3N_4 membrane grids for STEM analysis can be generally applied to a variety of nanolithography systems. By precise controlling of nanometre scale line widths further advancement can be made in making molecular contacts, or to produce spatially well defined areas as nucleation sites for bottom-up growth architectures.

Acknowledgments

The authors thank Rodney Andrews and Dali Qian of the Center for Applied Energy Research (University of Kentucky) for supplying MWCNTs and Alan Dozier for aid with TEM analysis. The Center for Micro-Magnetic Electronic Devices and the Electron Microscopy Center at the University of Kentucky provided critical equipment infrastructure. Sponsorship was provided by the Air Force Office of Scientific Research (DEPSCoR programme) under agreement No F49620-02-1-0225, Kentucky Science and Engineering Foundation grant No 148-502-03-49, and the Department of Energy Office of Science grant No DE-FG02-97ER45653.

References

[1] Miyazaki T, Kobayashi K, Yamada H, Horiuchi T and Matsushige K 2002 *Japan. J. Appl. Phys.* 1 **41** 4948
[2] Ito T and Okazaki S 2000 *Nature* **406** 1027
[3] Wallraff G M and Hinsberg W D 1999 *Chem. Rev.* **99** 1801
[4] Park J *et al* 2002 *Nature* **417** 722
[5] Bezryadin A and Dekker C 1997 *J. Vac. Sci. Technol.* B **15** 793
[6] Lefebvre J, Radosavljevic M and Johnson A T 2000 *Appl. Phys. Lett.* **76** 3828
[7] Xu T and Metzger R M 2002 *Nano Lett.* **2** 1061
[8] Chopra N, Andrews R, Xu W, Delong L and Hinds B J 2003 *Mater. Res. Soc. Symp. Proc.* **EXS 2** M5.4
[9] Chung J H, Lee K H and Lee J H 2003 *Nano Lett.* **3** 1029
[10] Chung J and Lee J 2003 *Sensors Actuators* A **104** 229
[11] Chen Z, Hu W, Guo J and Saito K 2004 *J. Vac. Sci. Technol.* B **22** 776
[12] Sorden R, Burghard M and Kern K 2001 *Appl. Phys. Lett.* **79** 2073
[13] Ancona M G, Kooi S E, Kruppa W, Snow A W, Foos E E, Whitman L J, Park D and Shirey L 2003 *Nano Lett.* **3** 135
[14] Kosiorek A, Kandulski W, Chudzinski P, Kempa K and Giersig M 2004 *Nano Lett.* **4** 1359
[15] Reed M A, Zhou C, Muller C J, Burgin T P and Tour J M 1997 *Science* **278** 252
[16] Chopra N, Kichambare P D, Andrews R and Hinds B J 2002 *Nano Lett.* **2** 1177
[17] Chopra N and Hinds B J 2004 *Inorg. Chem. Acta* **357** 3920
[18] Franklin N R and Dai H J 2000 *Adv. Mater.* **12** 890
[19] Weiss P S and Eigler D M 1992 *Phys. Rev. Lett.* **69** 2240
[20] Voigtlander B and Kastner M 2000 *Surf. Sci.* **464** 131
[21] Andrews R, Jacques D, Qian D L and Rantell T 2002 *Acc. Chem. Res.* **35** 1008
[22] Islam M F, Rojas E, Bergey D M, Johnson A T and Yodh A G 2003 *Nano Lett.* **3** 269
[23] Morikawa H, Kokura M, Iwatsu F and Terao T 1995 *Thin Solid Films* **254** 103